Available online at www.sciencedirect.com
SCIENCE DIRECT
International Journal of Heat and Fluid Flow 27 (2006) 551–557
International Journal of HEAT AND FLUID FLOW
www.elsevier.com/locate/ijhff

LES of open rotor–stator flow

Helge I. Andersson *, Magne Lygren [1]

Department of Energy and Process Engineering, Norwegian University of Science and Technology, 7491 Trondheim, Norway

Available online 3 May 2006

Abstract

Computer experiments (LES) of the axisymmetric and statistically steady turbulent flow between a rotating and a fixed disk have been performed. This flow is a representative of the flow in an unshrouded rotor–stator configuration. The flow is characterized only by a local Reynolds number and a local gap ratio, provided that the distance from the rotation axis is sufficiently large so that the flow is fully turbulent.

Five different cases have been considered, two of which may be classified as 'wide-gap' simulations, whereas the others were 'narrow-gap' simulations. In the latter cases, the variation of the tangential mean flow between the disks closely resembled the S-shaped mean velocity profile in a turbulent Couette flow. In the wide-gap cases, however, a nearly homogeneous core region separated the three-dimensional boundary layers adjacent to the rotor and the stator.

It was observed that the degree of three-dimensionality was gradually reduced with the distance from the axis of rotation. The Reynolds shear stress vector and the mean velocity gradient vector (both in planes perpendicular to the axis of rotation) became more aligned and the structural parameter increased towards the typical limit 0.15 found in two-dimensional boundary layers. The moment coefficient C_θ deduced from the statistically averaged tangential wall-friction at the rotor compared excellently with empirical correlation formulae, whereas C_θ at the stator side was substantially lower.

Keywords: Turbulence; Rotating disk; Large-eddy simulation; Three-dimensional boundary layers

1. Introduction

The axisymmetric and statistically steady turbulent flow between a rotating and a fixed disk is a representative of the flow in unshrouded rotor–stator configurations. This flow is among the canonical flows in which three-dimensional boundary layers can be subjected to in-depth explorations, see e.g. the recent review by Johnston and Flack (1996). However, besides its importance from a fundamental point of view, rotor–stator flows are of great practical concern in turbomachinery applications. A comprehensive treatise on flow over free disks in open and closed rotor–stator configurations was presented by Owen and Rogers (1989). Of particular concern for the present study are the findings of Daily and Nece (1960) in their experimental investigation of confined rotor–stator flow. They identified four different flow regimes, depending on the speed of rotation and the gap width, in which the flow was either laminar or turbulent and the boundary layers near the disks were either separated or merged. It is also well established that the flow is laminar near the axis of rotation and that transition to turbulence takes place at a certain radial position. Moreover, fully turbulent flow is found at smaller radii near the stator than at the rotor side.

This paper reports on an investigation of the flow sufficiently far away from the axis of rotation so that the flow is fully turbulent, i.e. beyond the transition zone, both on the stator and the rotor side. At a given location defined by the distance from the axis of rotation, the flow is characterized by a local Reynolds number and a local gap ratio. The objective of this computational study is to explore how these two independent parameters affect the three-dimensional mean flow and the turbulence statistics in an open rotor–stator configuration. The flow field near the rotating

* Corresponding author. Tel.: +47 73 59 35 56; fax: +47 73 59 34 91.
E-mail address: helge.i.andersson@ntnu.no (H.I. Andersson).
[1] Present address: STATOIL, Forusbeen 50, 4035 Stavanger, Norway.

0142-727X/$ - see front matter © 2006 Elsevier Inc. All rights reserved.
doi:10.1016/j.ijheatfluidflow.2006.02.030

disk can be anticipated to resemble the flow in a confined rotor–stator configuration studied experimentally by Itoh et al. (1992) and Itoh (1995). The present large-eddy simulations (LES) represent a continuation of the earlier DNS study reported by Lygren and Andersson (2001, 2002). They considered a narrow-gap case and compared their DNS results with experimental data of Itoh (1995). In the present study, a particular parameter combination is considered, which matches the laboratory experiment of Itoh et al. (1992), with which comparisons will be made.

2. Problem formulation

We consider the shear-driven motion of an incompressible Newtonian fluid between two parallel disks separated by a distance s, as depicted in Fig. 1. The lower disk (rotor) at $z = 0$ is rotating with a constant angular velocity ω, whereas the upper disk (stator) at $z = s$ is fixed. At a given location defined by the distance r from the axis of rotation, the flow is characterized by the local Reynolds number $Re_r = r^2\omega/\nu$ and the local gap ratio $G_r = s/r$, where ν is the kinematic viscosity of the fluid. For the sake of affordability, the computational domain consisted of an angular section $\theta_2 - \theta_1$ between the radial surfaces r_1 and r_2. Here, the inner radius r_1 is sufficiently large so that the flow is turbulent throughout the computational domain.

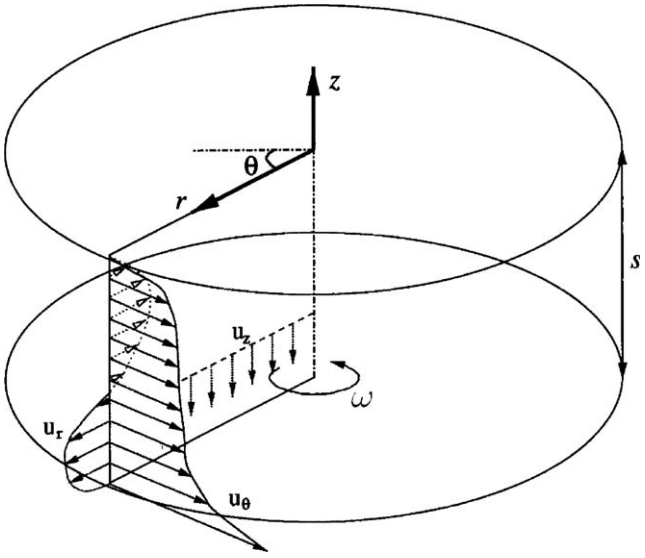

Fig. 1. Sketch of the flow configuration and coordinate system.

Altogether five different cases have been considered, i.e. five different combinations of the Reynolds number $Re_m = r_m^2\omega/\nu$ and the gap ratio $G_m = s/r_m$ based on the radial position $r_m = (r_1 + r_2)/2$ of the centre of the computational domain. One particular parameter combination was explored both by DNS (Case A1, Lygren and Andersson, 2001, 2002) and LES (Case A2, Lygren and Andersson, 2004), while only LESs were performed for the other cases, see Table 1.

3. Numerical approach

The three-dimensional Navier–Stokes equations were approximated by second-order accurate central-differences on a staggered grid arrangement and the flow field was advanced explicitly in time using a fractional-step technique and second-order accurate Adams-Bashforth time stepping. The computer code used was originally developed by Gavrilakis et al. (1986). In the course of the present study, the code was recast from Cartesian to cylindrical coordinates. Moreover, the original Poisson solver for the pressure field was replaced by a multigrid technique using repeated V-cycles and Line-Zebra Gauss–Seidel smoothening; cf. Andersson et al. (1998).

No-slip conditions were imposed at the stationary and the rotating disks so that the near-wall regions were explicitly computed. Conventional periodic boundary conditions were employed in the tangential direction, whereas full periodicity could not be assumed in the radial direction. Here, we adopted a modified version of a scheme used by Wu and Squires (2000) in LES of flow over a rotating disk. Their scheme represents a simplification of the boundary treatment devised by Lund et al. (1998) in their simulation of spatially developing boundary layers. The quasi-periodicity imposed in the radial direction in the present study consisted of the following basic steps at each time level. First, the instantaneous velocity field was decomposed into mean and fluctuating parts, the latter being formed as the product of root-mean-square of the turbulent fluctuations (averaged in the tangential direction and time) and a time-dependent signal assumed to exhibit periodicity between the coordinate planes r_1 and r_2. Thereafter, the fluctuating signal was used to generate time-dependent

Table 1
Overview of cases considered, domain size and resolution

Cases	Re_m	G_m	$N_r \times N_\theta \times N_z$	L_r/s	L_θ/s	Δr^+	$(r_m\Delta\theta)^+$
A1	4×10^5	0.02	$192 \times 192 \times 128$	3.5	7.0	5	10
A2	4×10^5	0.02	$48 \times 96 \times 48$	3.5	14.0	20	40
B	1×10^6	0.01265	$64 \times 96 \times 64$	3.5	10.0	20	40
C	1.6×10^6	0.01	$64 \times 96 \times 64$	3.0	8.0	22	38
D	6.4×10^5	0.1	$128 \times 128 \times 128$	1.5	3.0	24	48
E	1.6×10^6	0.0632	$128 \times 128 \times 192$	1.0	2.0	22	44

Case A1 (DNS) has been reported by Lygren and Andersson (2001, 2002) and Case A2 (LES) has been reported and compared with Case A1 by Lygren and Andersson (2004).

velocity fields at r_1 and r_2 at the new time level. Finally, global mass conservation was assured by imposition of a zero-mass-flux constraint through the coordinate planes r_1 and r_2.

In large-eddy simulations, a priori unknown subgrid-scale stresses appear in the filtered equations governing the large-scale motions. The unresolved small-scale turbulence is therefore represented by a subgrid-scale (SGS) model. The eddy-viscosity type SGS model originally implemented in the computer code was here replaced by the dynamic SGS model proposed by Lilly (1992) and the mixed dynamic model due to Vreman et al. (1994). A common feature of these SGS models is that the so-called Smagorinsky coefficient C_s is evaluated as a part of the solution rather than being a prescribed constant. See Lygren and Andersson (2004) for details. In that comparative study it was concluded that the best overall results were obtained with the mixed dynamic SGS model due to Vreman et al. (1994). That model has therefore been adopted in the present parameter study.

For all cases considered, the parameter values, the size of the computational domain, and the numerical resolution are summarized in Table 1. Here, L_r and $L_\theta = r_m(\theta_2 - \theta_1)$ denote the length of the domain in the radial and tangential directions, respectively, and N_i is the number of grid points in the x_i-direction. In an attempt to achieve about the same spatial resolution in all cases considered, the grid spacings in wall units were about 40×20 in the θ- and r-directions. The grid points next to the disks were about 0.5 wall units away from the surface, whereas Δz^+ was about 10 in the core region in Cases A–C and somewhat larger in Cases D and E.

In order to justify the length L_θ of the calculation domain, two-point correlations of the velocity fluctuations both near the rotor and the stator were provided by Lygren and Andersson (2001). These correlations became practically negligible at large separations and it was therefore concluded that the tangential extent of the computational domain was sufficiently large for Case A1. In that particular case, the tangential length L_θ^+ in wall units was 1860 on the rotor side and 1495 on the stator side. The difference is due to differences in the wall-friction velocity u_* based on the tangential component of the skin-friction vector τ_θ. For Case E, in which L_θ is only two times the gap width s, L_θ^+ is 5712 and 5128 on the rotor and stator sides, respectively. Since the elongated near-wall coherent flow structures scale on wall units, the extent of the computational domain can therefore be considered as fully satisfactory.

4. Results and discussion

The two controlling parameters Re_m and G_m can be combined into the gap Reynolds number

$$Re_G \equiv s^2\omega/\nu = G_m^2 \cdot Re_m \tag{1}$$

Table 2 shows that Re_G effectively distinguishes between narrow-gap Cases (A–C) and wide-gap Cases (D, E). This table also includes the Reynolds number based on the gap width s and the tangential wall-friction velocity $u_* = (\tau_\theta/\rho)^{1/2}$ at the rotating (Re_R^*) and the fixed (Re_S^*) disks. Here, τ_θ denotes the tangential component of the skin-friction vector, i.e. $\tau_\theta = -\mu\partial U_\theta/\partial z$, and should be evaluated either at the rotor (R) or at the stator (S). The narrow-gap Case A corresponds to the experimental study of Itoh (1995) and comparisons between DNS data and the laboratory measurements were made by Lygren and Andersson (2001). The LES of Case A2 was extensively compared with the DNS of Case A1 by Lygren and Andersson (2004). The wide-gap Case D corresponds to the case studied by Itoh et al. (1992) and comparisons will be made herein.

The tangential and radial mean velocity components are shown for Cases A–C in Fig. 2 and Cases D, E in Fig. 3. Profiles for the laminar case are included for comparative purposes. The former cases are considered as 'narrow-gap' cases with $Re_G = 160$ (see Table 2), and the tangential mean velocity exhibits an S-shaped profile similar to that in

Table 2
Wall-friction Reynolds numbers Re_R^* and Re_S^* based on the tangential wall-friction velocity at the rotor (R) and stator (S)

Cases	G_m	Re_G	Re_R^*	Re_S^*
A1	0.02	160	265.7	213.5
A2	0.02	160	267.7	214.3
B	0.01265	160	381	349
C	0.01	160	460	426
D	0.1	6400	2050	1534
E	0.0632	6400	2856	2564

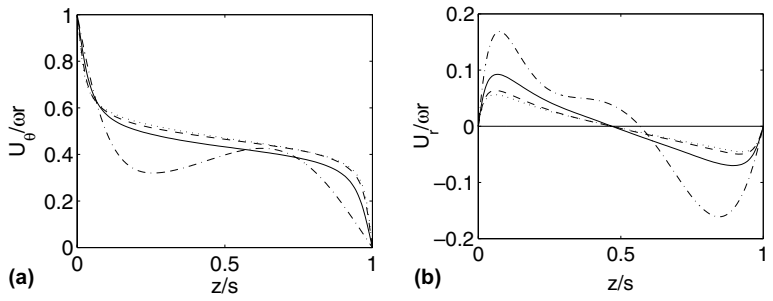

Fig. 2. Mean velocity components in tangential (a) and radial (b) direction in the narrow-gap cases. Laminar flow: chain-dotted line; Case A2: solid line; Case B: broken line; Case C: dotted line.

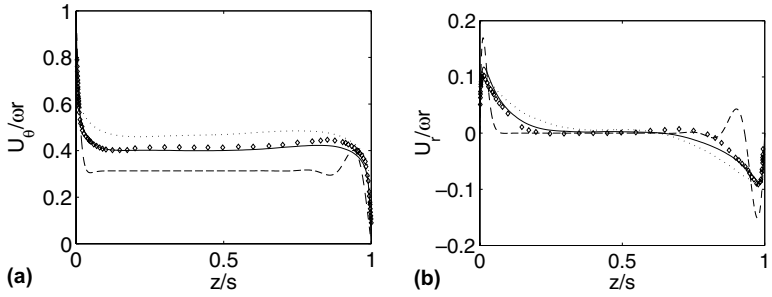

Fig. 3. Mean velocity components in tangential (a) and radial (b) direction in the wide-gap cases. Laminar flow: broken line, Case D: solid line; Case E: dotted line; symbols from Itoh et al. (1992).

plane turbulent Couette flow (Bech et al., 1995). In the 'wide-gap' cases in Fig. 3, on the other hand, $Re_G = 6400$ and a nearly homogeneous core region separates the three-dimensional boundary layers adjacent to the rotor and stator. Such flow configurations are known as Batchelor-type flow (Batchelor, 1951).

Since the gap Reynolds number Re_G defined in Eq. (1) is the same in the three narrow-gap simulations, they represent one and the same flow configuration but with the focus of attention (i.e. the computational domain) located 1.58 (Case B) and 2.0 (Case C) times further away from the axis of rotation than in Case A. Similarly, the computational domain in Case E is located 1.58 times further away from the z-axis than that of Case D. Here, it is worthwhile to recall that the present two-parameter problem can be recast into a one-parameter problem in Re_G for laminar flow situations, see e.g. Batchelor (1951). However, irrespective of whether the flow is laminar or turbulent, the fluid near the rotating disk is driven away from the axis of rotation ($U_r > 0$) due to centrifugal acceleration and this radial outflow along the rotor is compensated by flow directed towards the z-axis ($U_r < 0$) at the stator side (see Fig. 1).

It is noteworthy that the tangential velocity U_θ is consistently below $0.5\omega r$ midway between the disks. In the narrow-gap cases, $U_\theta/\omega r$ is 0.43, 0.46 and 0.47 in the three different cases and thereby tended towards the plane Couette flow value 0.50 with increasing Re_m. The profiles of U_r in Fig. 2(b) show that the cross-flow is substantially weaker than in the laminar case and reduces with increasing Re_m. The reduced three-dimensionality is also reflected by the data in Table 2, i.e. the wall-friction Reynolds numbers at the two disks become gradually closer to each other at the higher Re_m. In the wide-gap Cases D and E the core velocity was about $0.40\omega r$ and $0.47\omega r$, i.e. substantially larger than $0.31\omega r$ in the laminar case. It is also encouraging to observe from Fig. 3 that the LES results (Case D) compare reasonably well with the experiments of Itoh et al. (1992).

Even for a fixed gap Reynolds number Re_G, the flow field is affected by the local Reynolds number Re_m. Let us for example consider the structural parameter $a_1 = \tau/2k$, where τ denotes the magnitude of the turbulent shear stress vector in the (r,θ)-plane and k is the mean turbulent kinetic energy. Thus, $\tau = (\overline{u_\theta u_z}^2 + \overline{u_r u_z}^2)^{1/2}$ in the present context. z^+_{rel} denotes the distance to the nearest disk, scaled with the tangential wall-friction velocity u_* at that disk. The results in Figs. 4 and 5 show that a_1 approaches the standard value 0.15 for two-dimensional boundary layers away from the disks, except for the lowest Reynolds number Cases A and D, for which considerably lower values are observed. The same observations are made both in the narrow-gap and the wide-gap simulations. The observed reduction of a_1 indicates that rotor–stator flow is less efficient in extracting turbulence energy from the mean flow than 2D boundary layers.

Alternative measures of the mean flow skewness are the angle between the mean velocity gradient vector $(\partial U_\theta/\partial z, \partial U_r/\partial z)$ and the angle between the shear stress vector $(\overline{u_\theta u_z}, \overline{u_r u_z})$ and the tangential direction, respectively. These angles are shown in Fig. 6 for the three 'narrow-gap' cases, i.e. Cases A–C, for which $Re_G = 160$. These angles are seen to decrease with increasing value of the local Reynolds number both at the rotating and the stationary disk. This reflects that the mean flow is gradually becoming more aligned with the tangential direction.

The dotted lines in Fig. 6 represent the misalignment of the mean velocity gradient vector with the shear stress vector. A substantial misalignment of about 20° is observed in the immediate vicinity of the disks as well as far beyond the buffer region. Since isotropic eddy viscosity models rely on a perfect alignment of the shear stress vector with the velocity gradient vector, such closures are likely to fail in rotor–stator flows. It is noteworthy that this misalignment persists also at the higher Re_m Cases B and C, even though the structure parameter a_1 attains its conventional value 0.15 in these cases; cf. Fig. 4. Similar observations were made also for the wide-gap Cases D and E (not shown here).

The tangential component of the skin-friction vector τ_θ is directly responsible for the torque exerted by the fluid on the two disks. According to the Reynolds numbers based on the wall-friction in Table 2, the tangential component of the wall friction on the rotating disk (rotor) is generally higher than on the fixed disk (stator). Daily and Nece (1960) provided an empirical correlation for the torque coefficient for narrow-gap cases. From that correlation

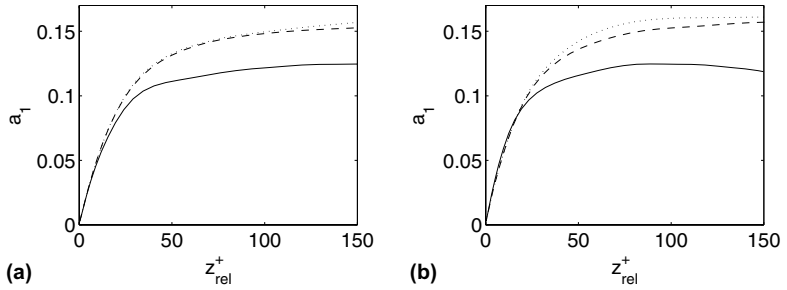

Fig. 4. Structural parameter $a_1 = \tau/2k$ in the narrow-gap cases. Rotor (a) and stator (b) side. Legend as in Fig. 2.

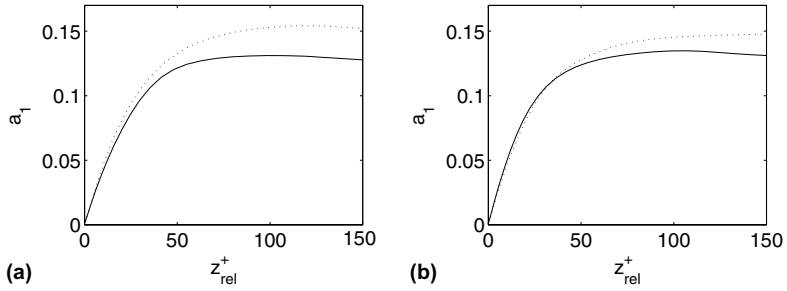

Fig. 5. Structural parameter $a_1 = \tau/2k$ in the wide-gap cases. Rotor (a) and stator (b) side. Legend as in Fig. 3.

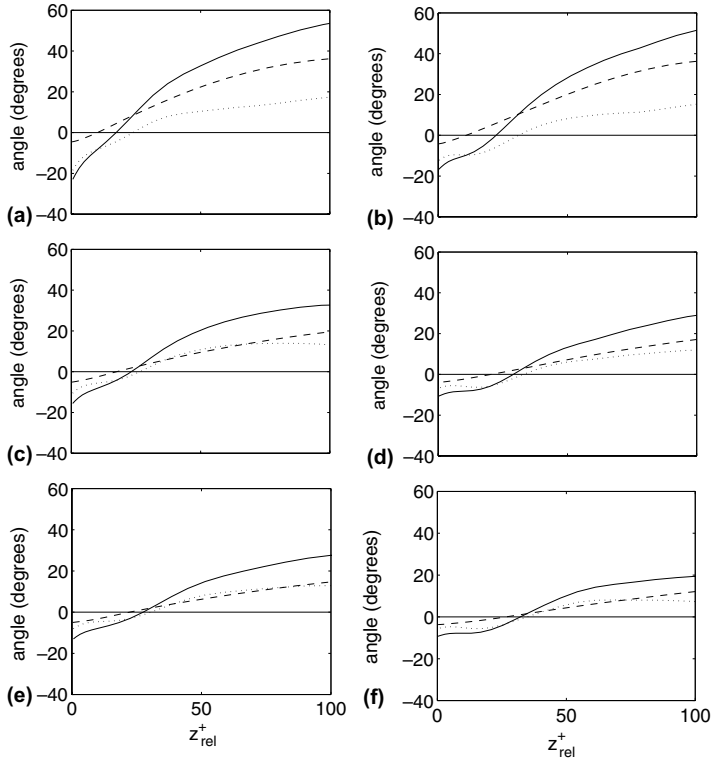

Fig. 6. Mean gradient angle (solid lines); shear stress angle (broken lines); difference (dotted lines). Rotor side (left) and stator side (right). Case A2: (a) and (b); Case B: (c) and (d); Case C: (e) and (f).

the following correlation for the skin-friction drag coefficient $C_\theta = 2\tau_\theta/\rho(r\omega)^2$ can be deduced:

$$C_\theta = 0.0298 G_r^{-1/6} Re_r^{-1/4} \quad (2)$$

Here, Re_r and G_r denote local Reynolds number and gap ratio (see Section 2). Similarly, the correlation

$$C_\theta = 0.0365 G_r^{1/10} Re_r^{-1/5} \quad (3)$$

can be derived from the empirical correlation for the torque coefficient provided by Daily and Nece (1960) for wide-gap cases. Here, it should be recalled that Daily and Nece (1960) measured the torque M on a disk which rotated within a chamber. Their frictional torque thus arose from the wall-friction exerted by the fluid on both sides of the rotor. Therefore, the accompanying wall-friction τ_θ can be deduced by differentiating their M with respect to r (and divide by 2). In this way, Eqs. (2) and (3) have been deduced from Eqs. (46) and (47) in Daily and Nece (1960). First, however, the numerical coefficient 0.0102 in Eq. (47) was multiplied by a factor 10 to make their correlation consistent with the data points in their Fig. 5(a). Since the local gap ratio according to Eq. (1) is given as $G_r = Re_G^{1/2} Re_r^{-1/2}$ and Re_G is fixed both for the narrow-gap cases ($Re_G = 160$) and the wide-gap cases ($Re_G = 6400$), C_θ should vary as $Re_r^{-1/6}$ in the narrow-gap cases according to Eq. (2) and as $Re_r^{-1/4}$ in the wide-gap cases according to Eq. (3).

The skin-friction drag coefficient C_θ can readily be deduced from the LES since

$$C_\theta = 2(u_*/r\omega)^2 = 2(Re^*/G_r Re_r)^2 \tag{4}$$

where Re^* is given in Table 2 for all the cases considered. The correlation (2) is shown in Fig. 7 together with the present LES data. The wall friction at the rotor (stars) closely follows the empirical line (2), whereas the flow resistance turns out to be lower at the stator side (squares). It can be anticipated that the radial mean velocity component U_r will be further reduced at even higher Re_r and the friction at the two disks will eventually become equal. The LES data for the wide-gap cases in Fig. 8 show a somewhat bigger difference between the rotor and the stator, in accordance with the experimental data of Itoh et al. (1992).

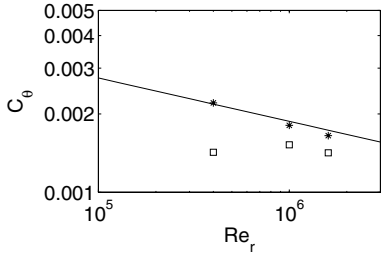

Fig. 7. Friction factor at the rotor (*) and stator (□) Cases A2, B and C. Eq. (2): solid line. $Re_G = 160$.

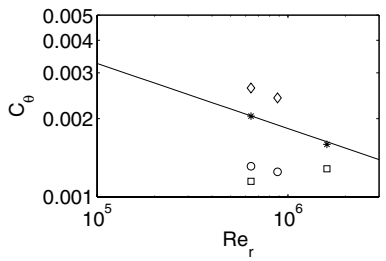

Fig. 8. Friction factor at the rotor (*) and stator (□) Cases D and E. Eq. (3): solid line. $Re_G = 6400$. Data from Itoh et al. (1992): rotor (◊) and stator (○).

5. Concluding remarks

This parameter study has demonstrated the distinguishing features of narrow-gap and wide-gap rotor–stator configurations. In spite of the fundamentally different core regions, the three-dimensional flow fields in the vicinity of the two disks exhibit the same general features in all cases considered. It is remarkable that the misalignment of the shear stress vector with the velocity gradient vector persisted even when the structural parameter attained its typical value 0.15 routinely found in 2D flow configurations.

The present study supports the view advocated by Littell and Eaton (1994) that the mean flow three-dimensionality affects the near-wall vortices and their ability to generate shear stresses. This conclusion applies both for the narrow-gap and the wide-gap cases. The difference between the rotor and the stator sides diminishes with increasing local Reynolds number. A separate analysis of conditionally averaged shear stresses (Andersson and Lygren, 2002) supports these findings.

Acknowledgements

The authors are grateful to an anonymous referee whose constructive comments helped to improve the paper. The second author was the recipient of a research fellowship offered by the Research Council of Norway under Contract No. 115548/410. Computing time on CRAY J90 was also provided by the Research Council of Norway (Programme for Supercomputing). Professor M. Itoh (Nagoya Institute of Technology) generously made available his experimental data.

References

Andersson, H.I., Lygren, M., 2002. Coherent structures in 3D mean flow. In: Castro, I.P. et al. (Eds.), Advances in Turbulence IX. CIMNE, pp. 649–652.

Andersson, H.I., Lygren, M., Kristoffersen, R., 1998. Roll cells in turbulent plane Couette flow: reality or artifact? In: Bruneau, C.H. (Ed.), 16th International Conference on Numerical Methods in Fluid Dynamics. Springer, pp. 117–122.

Batchelor, G.K., 1951. Note on a class of solutions of the Navier–Stokes equations representing steady rotationally-symmetric flow. Quarterly Journal of Mechanics and Applied Mathematics 4, 29–41.

Bech, K.H., Tillmark, N., Alfredsson, P.H., Andersson, H.I., 1995. An investigation of turbulent plane Couette flow at low Reynolds numbers. Journal of Fluid Mechanics 286, 291–325.

Daily, J.W., Nece, R.E., 1960. Chamber dimension effects on induced flow and frictional resistance of enclosed rotating disks. Journal of Basic Engineering 82, 217–232.

Gavrilakis, S., Tsai, H.M., Voke, P.R., Leslie, D.C., 1986. Large-eddy simulation of low Reynolds number channel flow by spectral and finite difference methods. In: Schumann, U., Friedrich, R. (Eds.), Notes on Numerical Fluid Mechanics, vol. 15. Vieweg, pp. 105–118.

Itoh, M., 1995. Experiments on the turbulent flow in the narrow clearance between a rotating and a stationary disk. In: Carrol, B.F. et al. (Eds.), Turbulent Flows, vol. 208. ASME-FED, pp. 27–32.

Itoh, M., Yamada, Y., Imao, S., Gonda, M., 1992. Experiments on turbulent flow due to an enclosed rotating disk. Experimental Thermal and Fluid Science 5, 359–368.

Johnston, J.P., Flack, K.A., 1996. Review – advances in three-dimensional turbulent boundary layers with emphasis on the wall-layer regions. ASME Journal of Fluids Engineering 118, 219–232.

Lilly, D.K., 1992. A proposed modification of the Germano subgrid-scale closure method. Physics of Fluids A4, 633–635.

Littell, H.S., Eaton, J.K., 1994. Turbulence characteristics of the boundary layer on a rotating disk. Journal of Fluid Mechanics 266, 175–207.

Lund, T.S., Wu, X., Squires, K.D., 1998. Generation of turbulent inflow data for spatially developing boundary layer simulations. Journal of Computational Physics 140, 233–258.

Lygren, M., Andersson, H.I., 2001. Turbulent flow between a rotating and a stationary disk. Journal of Fluid Mechanics 426, 297–326.

Lygren, M., Andersson, H.I., 2002. Turbulence statistics in an open rotor–stator configuration. Physics of Fluids 14, 1137–1145.

Lygren, M., Andersson, H.I., 2004. Large eddy simulations of the turbulent flow between a rotating and a stationary disk. Zeitschrift für angewandte Mathematik und Physik 55, 268–281. First version in: Lindborg, E. et al. (Eds.), Proceedings 2nd International Symposium on Turbulence and Shear Flow Phenomena, KTH, Stockholm, 2001, pp. 407–412.

Owen, J.M., Rogers, R.H., 1989. Flow and Heat Transfer in Rotating-Disk Systems: Rotor–Stator Systems. Research Studies Press, Taunton, NY.

Vreman, B., Geurts, B., Kuerten, H., 1994. On the formulation of the dynamic mixed subgrid-scale model. Physics of Fluids 6, 4057–4059.

Wu, X., Squires, K.D., 2000. Prediction and investigation of the turbulent flow over a rotating disk. Journal of Fluid Mechanics 418, 231–264.